MNE 19 (2023) 100213

Contents lists available at ScienceDirect

Micro and Nano Engineering

journal homepage: www.sciencedirect.com/journal/micro-and-nano-engineering

Low-cost piezo-MEMS speaker technology

Sanjog Vilas Joshi [a,*], Sina Sadeghpour [a], Michael Kraft [a,b]

[a] Dept. of Electrical Engineering (ESAT-MNS), KU Leuven, Belgium
[b] Leuven Institute for Micro- and Nanoscale Integration (LIMNI), KU Leuven, Belgium

ARTICLE INFO

Keywords:
Piezoelectric thin films
PZT
Piezo-MEMS
MEMS speaker
Earphone

ABSTRACT

In this paper, we are reporting low-cost piezo-MEMS speakers based on an SOI-free process. The speaker membrane is made of a 1.5 μm thick polyimide passive layer, obviating the need for SOI wafers. The custom-made PZT solution for depositing 1 μm sol-gel PZT thin films has further reduced fabrication costs. The membranes are realized by a backside Deep Reactive Ion etching (DRIE) on the silicon wafer. Laser doppler vibrometer (LDV) characterization has shown the resonance frequency of a single speaker element with a diameter of 2.5 mm to be 30 kHz with a sensitivity of 100 mm/s/V, whereas sensitivity at 4 kHz is around 1.2 mm/S/V. The speaker element can produce around 70–90 dB in-ear Sound Pressure Level (SPL) response in audible frequencies (100 Hz – 10 kHz) at 5 V excitation as shown by a simulation in an ear-coupler which is in line with the LDV measurements. Moreover, on average, the fabricated 4 × 4 arrays have shown a 10 dB higher SPL than a single-speaker element as measured by a microphone.

1. Introduction

With the development of portable devices and wearable electronics, there are increasing requirements for the miniaturization and integration of electronic devices, including a need for smaller and more energy-efficient speakers. MEMS (Micro-electro-mechanical systems) speakers have a small form factor and high compatibility for mass production with reduced power consumption [1]. Previously reported MEMS speakers mostly adapted electrostatic actuation due to their simple structure and compatibility with a standard CMOS process. However, electrostatically actuated MEMS speakers can hardly produce high output pressure and require a high operating voltage [2]. Electromagnetic speakers can generate a high sound pressure without a high voltage than electrostatic speakers. However, the required magnet leads to complicated microfabrication and packaging of the device [3].

Recently, piezoelectric thin-film actuation has become more popular due to low actuation voltage and higher actuation force [4]. This makes it a good candidate for a variety of MEMS devices and applications, including ink-jet printer heads [5], MEMS scanning mirrors [6], ultrasonic motors [7], RF resonators [8], and acoustic generators [9]. Also, piezo-electric thin films in MEMS speakers have demonstrated satisfactory sound pressure levels (SPLs) at relatively low voltages [1] and there is a growing trend of piezoelectric MEMS speakers with high SPLs of 80 dB or above due to the requirements in mobile phones, wearables, IoT devices, earphones, hearing instruments, and portable electronic and music devices. However, note that the SPLs comfortable for humans is about 60 to 65 dB and any sound above 80 dB is harmful; and for a special case of in-ear applications, the closed volume defined by the ear canal amplifies the sound below 4 kHz by 10–20 dB before reaching the eardrum diminishing the need for large deflections of the speaker membranes [10].

The main component of our piezoelectric MEMS speakers is a vibrating membrane with a piezoelectric thin film. The membrane is driven by applying an excitation voltage between the top and bottom electrodes of the piezoelectric layer. The applied electric field forms transverse stress in the active piezoelectric layer, which causes out-of-plane membrane displacements generating a pressure wave in the outer medium. Moreover, membrane geometry can be freely chosen to provide sufficient output acoustic pressures at desirable frequencies [11]. In contrast to electrostatic technology, piezoelectric technology does not necessarily require a DC biasing voltage. However, the downside of piezo-based designs is the low electro-mechanical coupling coefficients limited by piezoelectric thin film properties, which results in lower bandwidth. Also, typical materials used in the fabrication of piezoelectric actuators, AlN and PVDF have a weaker e_{31} piezoelectric coefficient compared with PZT, which results in a low transmit sensitivity even at the resonance frequency [12,13].

This paper reports PZT thin film actuated speakers with a strong

* Corresponding author.
E-mail address: sanjogvilas.joshi@kuleuven.be (S.V. Joshi).

https://doi.org/10.1016/j.mne.2023.100213
Received 9 January 2023; Received in revised form 18 May 2023; Accepted 9 June 2023
Available online 10 June 2023

piezoelectric effect to overcome the challenges associated with transmission response. PZT is a well-known material for piezo-MEMS applications with its excellent piezoelectric properties [14]. Our method benefits from an in-house PZT solution-making process and deposition procedures to reduce costs. For further cost reduction and simplicity, we have used conventional silicon wafers instead of SOI wafers (SOI technology is a convenient piezo-MEMS speaker fabrication technique because of the silicon device layer with a desired thickness, which makes it easy to realize the membranes [15]). Speakers fabricated on inexpensive silicon wafers with polyimide membranes present a low-cost alternative to SOI technology.

The operation of our speaker is evaluated with the characterizations in a free field with a microphone which are validated by simulations, theoretical calculations, and reported data. Furthermore, finite element simulations in an ear-coupler are presented and supported by membrane vibration measurements suggesting the suitability of the technology for in-ear applications. Also, the power consumption of our speaker is estimated and compared with that of the typical earphones in the market.

2. Device design

A single element of our proposed speaker consists of a polyimide membrane situated above the top electrode and the active piezoelectric (PZT) layer, as shown in Fig. 1a. Here, the polyimide passive layer arrangement in the membrane is different from the usual silicon passive layers in SOI technology. In an SOI device, active layers, such as the PZT thin film, are realized on top of the passive silicon device layer of the SOI wafer. By using polyimide, vibrations generated by the PZT layer are damped (polyimide, being a polymer, is associated with higher material damping coefficients or loss factors than PZT ceramic [16,17]), which helps in widening the bandwidth, as demonstrated in [18]. In this way, the resulting low Q factor is likely to distribute the energy better in the audible frequencies than in a high Q device. Additionally, the mass of the medium can effectively dampen the membrane vibration when the lateral dimension of the membrane is smaller than the wavelength, thus 2.5 mm is chosen as the diameter of the speaker [11].

The resonance frequency is designed to be around 25–30 kHz. Our design has a smaller form factor compared to the designs with lower resonance frequencies. The latter can have apertures twice as large as the one demonstrated in this paper [1]. Realizing thin membranes with large aperture sizes present challenges during microfabrication as they are more fragile whereas a thicker membrane design can result in costly production with reduced performance efficiency, as a higher force is required to vibrate a membrane with a heavier mass. Moreover, the smaller form factor makes our design more suitable for applications such as earphones. With a resonance frequency beyond the audible range, the high amplitude vibrations around resonance are not present in the audible frequency range. Also, the resonance frequency is not too far from the audible range, so the device would not witness significant attenuation of the wave pressure compared to pressure at resonance. Accordingly, a flatter SPL response at very low frequencies, as demonstrated in [19], is also witnessed in this work.

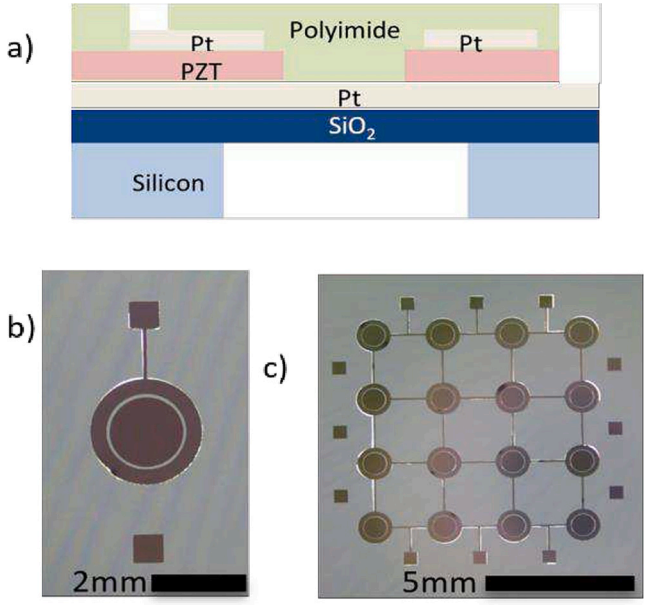

Fig. 1. (a) Schematic of a speaker element (not to scale). (b) 2.5 mm speaker element (c) 4 × 4 speaker array elements connected in parallel.

Fig. 1b shows the fabricated speaker element. The PZT and the top electrode are placed on the perimeter of the membrane covering a width of about 30% of the membrane diameter. As demonstrated by the simulation in Fig. 2b,c, this improves the vibration response by about 10% compared to the case with PZT everywhere in the membrane and the top electrode in the central 70% area. The improvement is due to the lower flexural rigidity of the membrane.

Along with the single speaker element, 4 × 4 arrays are also designed with 1.85 mm, 1.45 mm, and 1.25 mm single element diameters to compare the resonance frequencies and response in the audible range. The array elements are connected in parallel. Fig. 1c shows the design of the array with 1.25 mm-sized membranes.

3. Comsol simulations

The single-element speaker was simulated using a 2D axisymmetric model. The electrodes were not separately defined. PZT was actuated with a 0.25 V electric potential difference between the top and bottom boundaries with the electrostatics module of COMSOL. This setting has closely matched the performance of the fabricated pMUT when it is actuated with 5 V. The discrepancy in the voltage is due to the difference in the piezoelectric and elastic properties of the PZT in the fabricated and simulated device.

3.1. Eigenfrequency and vibration analysis

The thickness of the membrane passive layer i.e., polyimide, was tuned so that the eigenfrequency was around 30 kHz. The eigenfrequency simulation in Fig. 2a shows the speaker element structure with 30 μm polyimide having an eigenfrequency of about 30 kHz. Next, a frequency sweep was performed, and the in-air frequency response of the membrane displacement was determined in the ring electrode (Fig. 2b) as well as central electrode configuration (Fig. 2c). For this step, isotropic loss factor (0.06) damping was introduced in the solid mechanics model, defined by the reciprocal of twice the quality factor measured with an LDV [20].

After the eigenfrequency and vibration analysis, the acoustic pressure simulations for the single speaker element were followed. The simulated pressure response is especially useful for the understanding of acoustic device behavior at conditions where pressure measurements present limitations, such as 1) measurements at very low frequencies where the SNR is low, 2) prediction of response very close to the speaker surface where a microphone positioning can be difficult and thus cannot be precisely adjusted, and 3) for pressure field measurement in the ear which requires specialized couplers and microphones. On the other hand, a calibrated microphone allows the characterization of array devices that are difficult to accurately simulate.

3.2. Free field simulations

To start with, the free field pressure is simulated in the audible range by setting up an acoustic pressure module with a perfectly matching layer (PML). Fig. 3a shows pressure distribution at about 4 kHz due to

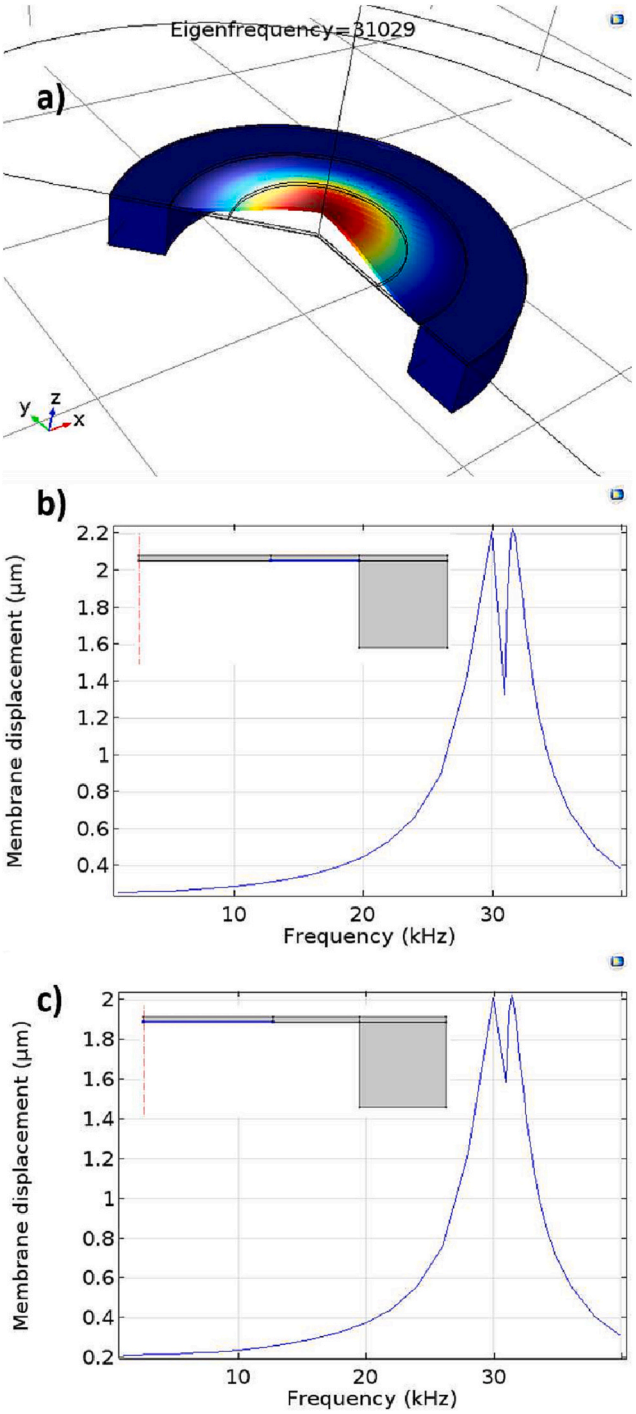

Fig. 2. (a) Simulated speaker element geometry with the indication of eigenfrequency. Membrane displacement (b) when PZT and top electrode form an outer ring (c) when PZT covers all area with the top electrode in the central 70% area. Inset shows the geometry with the blue line indicating actuated region. (For interpretation of the references to colour in this figure legend, the reader is referred to the web version of this article.)

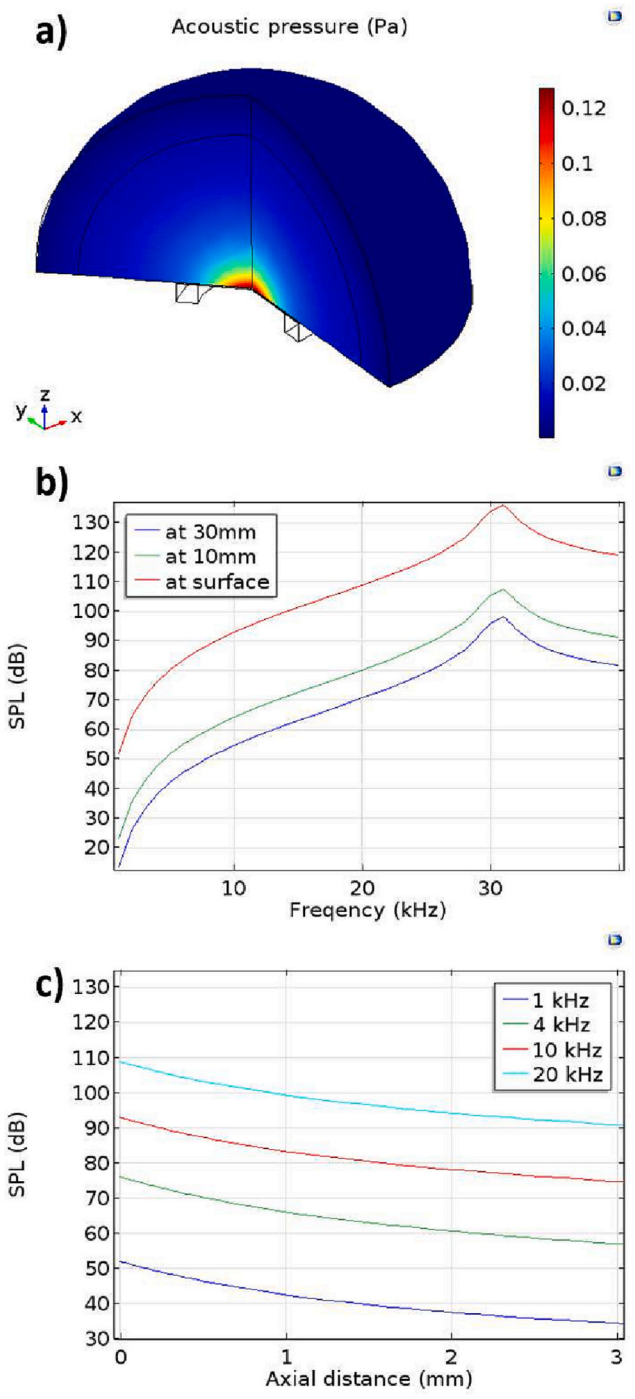

Fig. 3. (a) Pressure distribution in the free field (sphere with radius 5 mm) at 4 kHz due to 2.5 mm speaker element (b) SPL response of the speaker element with frequency. (c) SPL decrease with axial distance.

the 2.5 mm speaker element. SPL at the surface, at 1 cm (for validation with reported data), and at 3 cm (for comparison with experimental results) is plotted in Fig. 3b. It indicates that the speaker can produce 50–90 dB SPL in the 1–10 kHz range at the surface. However, SPL drops significantly at distances beyond 1 cm. Fig. 3c shows the SPL as a function of axial distance at 1 kHz and 4 kHz (mid-range frequencies in music) as well as at 10 kHz (treble frequency) and 20 kHz (uppermost limit of human hearing). It highlights that the SPL curve shifts downwards as lower frequencies are approached (the ones of interest in music). These simulations suggest that such design is not very suitable for a free-field loudspeaker.

3.3. *Pressure field simulations in an ear couplar*

In addition to free-field analysis, pressure field simulations with a generic 711 coupler were carried out to evaluate the viability of using our speaker in the context of an earphone application. The 711 coupler is an occluded ear-canal simulator that approximates the acoustic

impedance of the ear canal. The details of the model can be found in [21]. It is intended to have the same acoustic properties as the average occluded human ear-canal and eardrum system, approximately from the second bend in the ear canal to the eardrum. Besides certain details, the geometry corresponds to the Brüel & Kjær Ear Simulator Type 4157. An ear simulator enables the prediction of sound amplification and ear drum sound pressure. However, above 10 kHz, the 711 coupler does not simulate a human ear.

The 711 coupler model was extended by adding the design of our speaker at the input. The coupling of membrane displacement to the acoustic pressure in the ear canal cylinder is achieved using the normal displacement feature from pressure acoustics physics. The input normal displacement came from the z-displacement generated by coupled solid mechanics and the electrostatics model of the speaker. The inclusion of the side volumes and the slits on the cylinder surface mimicked the complex eardrum mechanical losses using an acoustic system. This model is set up using two different methods: 1) a model using thermo-viscous acoustics, and 2) a model with the narrow region acoustics feature in pressure acoustics. Again, the model details can be found in [21]. Both models show very similar responses in the intended 10 kHz range.

Fig. 4a shows the geometry of the coupler with the speaker membrane at the top and the eardrum at the bottom (modeled by applying RCL impedance feature in the pressure acoustics physics to the bottom surface where the R, C and L values were the default ones from the generic 711 coupler model from COMSOL application library). The same figure shows the acoustic pressure across the coupler volume (according to the thermoviscous model) at 4 kHz and is uniform around 80 dB or 0.2 Pa. Fig. 4b shows the ear simulator response from 100 Hz to 10 kHz. The inset shows the displacement of the membrane generated by this simulation model that closely agrees with the LDV data at 4 kHz (in Table 1 or Fig. 8b) and 2D simulation data in Fig. 2b with 5 V actuation. The sound pressure output generated by the acoustic diaphragm is proportional to vibration amplitude and area at a particular frequency [22]. As the simulated model generates membrane displacements (inset of Fig. 4b) that are in line with the ones measured in LDV data, one can estimate pressure levels (SPL) in response to the 5 V actuation of the fabricated device. The graph implies a flat SPL of 67 dB in the range of 100–700 Hz and a pseudo-static speaker dynamic behavior. As noted in the introduction, this is already a comfortable and safe SPL. To further improve the SPL in the sub-kHz range by 6–12 dB, instead of 5 V, voltages up to 10–20 V are recommended (Fig. 4b). Then, the performance is at par with the reported 85 dB response of a PZT-based speaker on an SOI wafer at 1 kHz measured with a standard ear simulator [14]. Fig. 4c shows the impedance of the ear canal which is seen to comply well with the IEC standards.

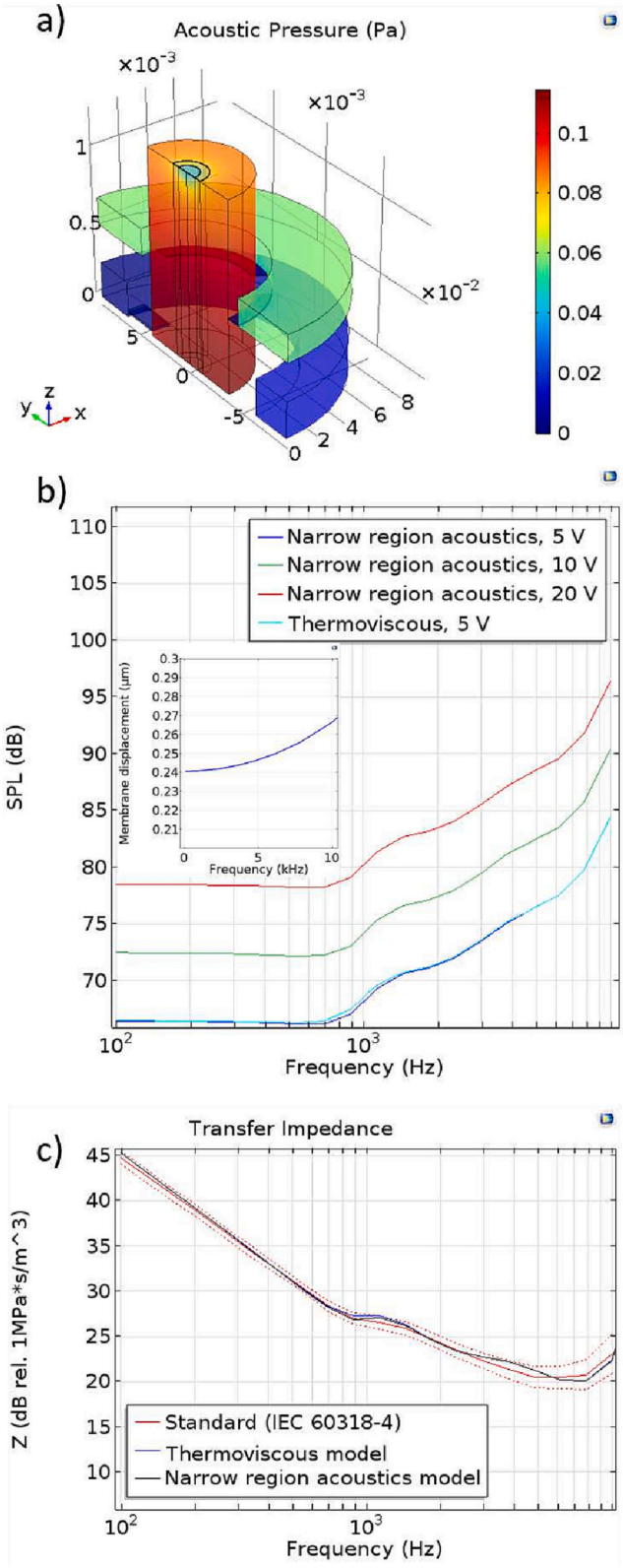

Fig. 4. (a) Pressure distribution inside the ear coupler volume at about 4 kHz. 2.5 mm speaker element at the top and eardrum at the bottom (b) SPL response of 2.5 mm speaker element at coupler microphone (eardrum) with 5, 10 and 20 V actuation. In the inset, membrane displacement at 5 V (c) Transfer impedance of the ear coupler system compared with IEC standards.

4. Materials and methods

4.1. PZT thin film process

Fig. 5 shows the sol-gel deposition method for PZT thin film used in the speaker fabrication. As a first step, a PZT stock solution was prepared. Lead acetate, zirconium propoxide (70 wt% solution in 1 - propanol), and titanium isopropoxide were used as precursors. Acetic acid, Acetylacetone, and Propylene Glycol were used as stabilizers and additives. Lastly, Methanol was used as a solvent. The sequence of the steps is described in Fig. 5 (top).

PZT thin film was deposited on top of the Pt bottom electrode with the procedure involving repeated spin coating, pyrolysis, and rapid thermal annealing (RTA), with the parameters described at the bottom of Fig. 5. Four iterations were performed to obtain 1 µm film.

4.2. Device fabrication

The 100-silicon wafer was cleaned with piranha and BHF followed

Table 1
Summary of LDV measurements.

Device type	Membrane Diameter (mm)	Resonance Frequency (Hz)	Transmit Sensitivity (mm/s/V)	
			at Resonance	at 4 kHz
Single Element	2.5	29,545	102.2	1.218
4 × 4 Array	1.85	57,036	3.432	0.1282
	1.45	70,367	6.99	0.1048
	1.25	89,523	10.08	0.0801

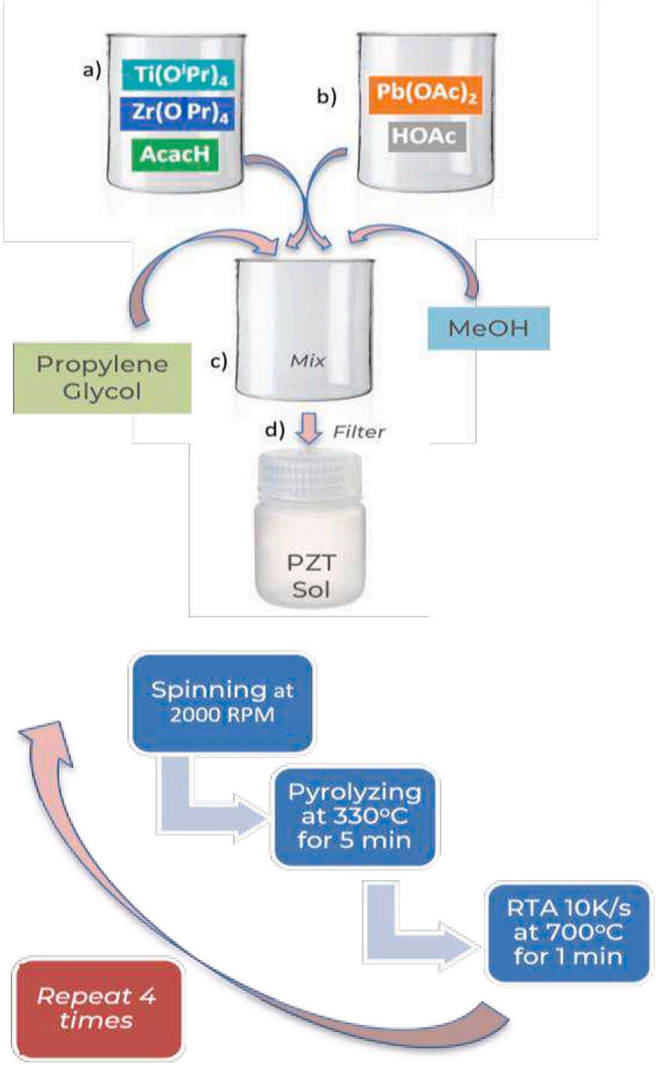

Fig. 5. Top: recipe of making PZT solution- (a) In a beaker, Zr and Ti precursors refluxed with Acetylacetone in stochiometric amounts. (b) In another beaker, 10% excess Pb precursor refluxed with acetic acid. (c) Two solutions were mixed with each other followed by addition of sol stabilizer and solvent. (d) The contents were allowed to mix and solution was filtered in a stock bottle. Bottom: PZT thin film deposition procedure- Spin coating, pyrolysis and RTA were repeated 4 times, in a cycle.

by wet oxidization in the oxidation oven. This resulted in 500 nm of oxide on both sides of the wafer. The oxide serves as etch stop in the final DRIE process. Next, about 200 nm Pt bottom electrode was sputtered with (111) orientation. Pt serves as a seed layer for the PZT deposition process.

Using the sol-gel method described in the previous subsection, 1 μm PZT was deposited on top of the Pt bottom electrode. PZT was patterned using a previously reported wet etching procedure in the center of the membrane forming a ring-shaped PZT on the membrane [23]. Patterning the PZT also gives access to the bottom electrode. Then, the top Pt electrode was patterned by the liftoff covering a ring-shaped PZT.

Once active layers were prepared, 1.5 μm polyimide (PI2611, HD Microsystems) was spun to serve as the membrane material and was patterned to access both electrode pads. This polyimide thickness is optimized experimentally during fabrication runs to obtain a 30 kHz resonance frequency for the single-element speaker with a membrane diameter of 2.5 mm. The thickness is different from the one used in the simulation (30 μm). It is supposedly because of the residual stress and stiffness of the polyimide, PZT, and remaining layers which are different in reality than in the simulation. Sadeghpour et al. have pointed out that the effect of the residual stress on the resonance is very pronounced at lower frequencies [11]. Finally, the wafer backside was patterned using DRIE to realize the membranes and complete the fabrication. The fabrication process flow is shown in Fig. 6.

5. Experimental results and discussion

5.1. Material and electrical characterization

To characterize the deposited PZT thin film, 1) XRD measurements after the PZT deposition and 2) P-E hysteresis loop measurements after the top electrode deposition were performed. (111)-orientated PZT without any pyrochlore phase (normally around 29°) was obtained according to the XRD results, as shown in Fig. 7a. Such a dominant crystal orientation is a confirmation to have a satisfactory d_{31} coefficient and transmission sensitivity in the deposited PZT layer.

A sawyer-tower circuit was used for the P-E hysteresis loop measurement. The PZT capacitor and the sample capacitor (C_o) of a known value were connected in series. The value of the sample capacitor (~30 times the PZT capacitance) was chosen such that almost 97% of the applied voltage dropped across the PZT capacitor. From the applied voltage signal, the electric field was calculated by considering the PZT thickness. Polarization charge density across the PZT capacitor was determined by dividing the charge across the sample capacitor, C_oV_o, (same as the charge across the PZT capacitor, being in series) by the area of the PZT capacitor. Remnant polarization and coercive field of 14 μc/cm2 and 50 kV/cm, respectively, compared well with recent reports (Fig. 7b) [24].

After the PZT material characterization, the capacitance of the single-element speaker device was measured to be 16 nF. The arrays with 1.25 mm, 1.45 mm and 1.85 mm diameter elements had capacitances of 87 nF, 126 nF, and 184 nF, respectively. The speaker element impedance showed a capacitive response and varied from 10,000 Ω to 500 Ω for frequencies 1 kHz - 20 kHz. The power consumption of the single element speaker at 1 kHz with 5 V actuation is estimated as 2.5 mW, comparing well with the typical earphones in the market- JBL C50HI with 3 mW rated and 10 mW peak power [25], Phillips TAE1107BK/94, 5 mW max power input [26]. However, the capacitive impedance of the technology demonstrated in this paper is higher and might need different driving electronics as opposed to the 32 Ω impedance standard in the market [27].

5.2. Vibration and acoustic pressure measurements

The electrical measurements were followed by the characterization of the vibration performance. With membrane-based piezo devices, an LDV can record the in-air frequency response. The transducer was excited with a periodic chirp signal applied over a band of frequencies, 10–37 kHz, to detect the resonance. Fig. 8a shows the frequency response of a single speaker element and the arrays measured with an LDV (Polytec MSA-600). The 2.5 mm single speaker element showed 30 kHz resonance according to the design and a quality factor of ~8–9.

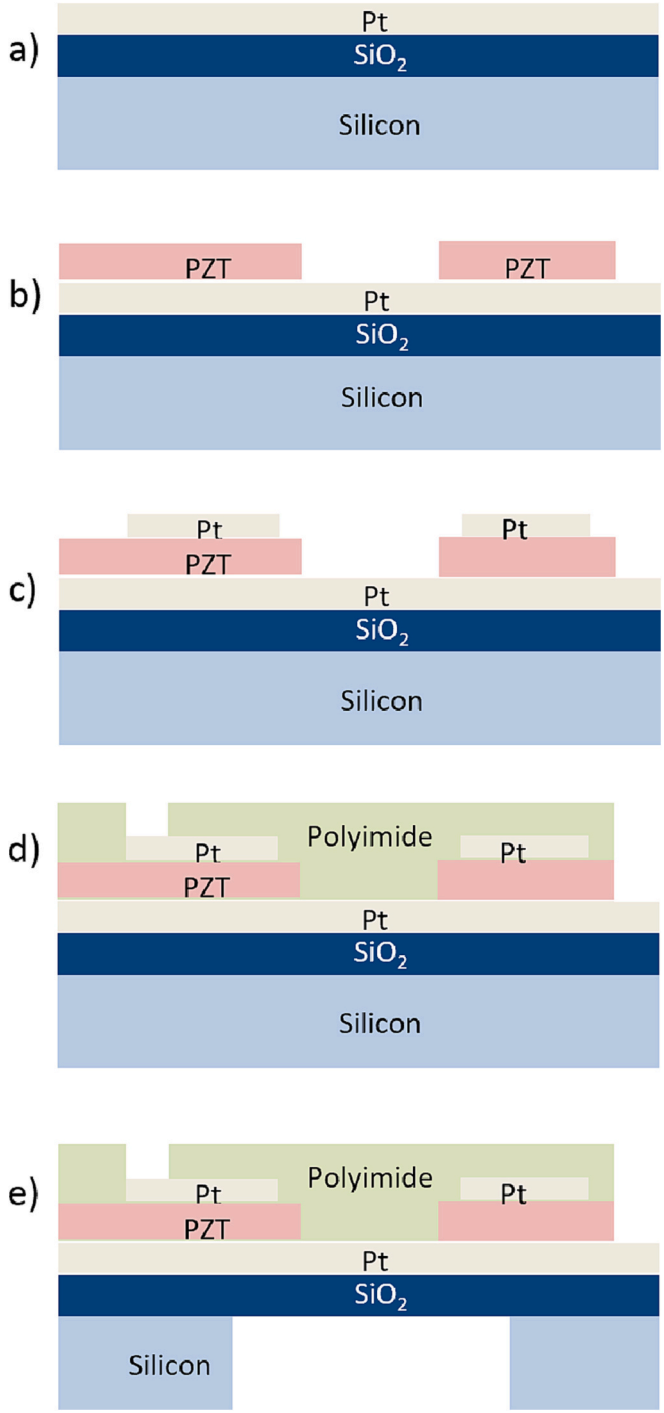

Fig. 6. Speaker device fabrication process- (a) Oxide growth followed by backside oxide removal and deposition of the Pt as the bottom electrode. (b) Deposition and patterning the PZT layer. (c) Patterning the top electrode. (d) Deposition and patterning the polyimide passive layer. (e) Realizing the membrane by DRIE.

Seven randomly selected elements from the array with 1.85 mm membrane diameter showed resonance frequencies of 56,108 Hz, 56,445 Hz, 56,821 Hz, 57,588 Hz, 57,036 Hz, 56,797 Hz, and 57,412 Hz, which indicated a 1.5% variation from the central 57 kHz frequency and confirmed good fabrication uniformity. The other arrays, with 1.45 mm and 1.25 mm membrane diameters showed resonance at 70 kHz and 90 kHz, respectively.

The sensitivity of the speakers at a particular frequency was

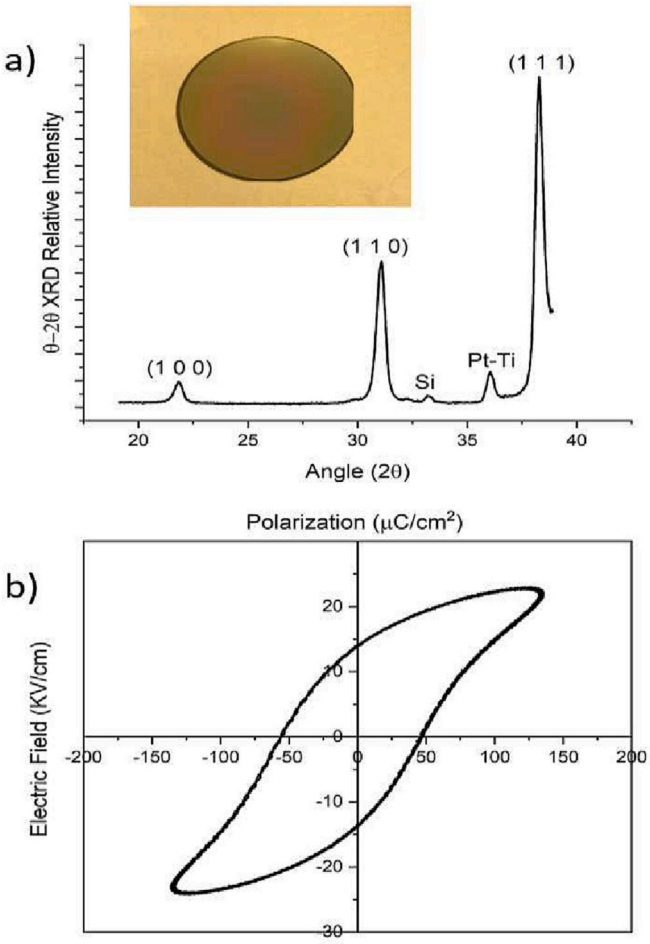

Fig. 7. (a) XRD showing (111) orientation (PZT wafer prepared for XRD in the inset), and (b) polarization vs. electric field (P-E) hysteresis loop at 1 kHz, of deposited PZT thin film.

measured with a sinewave excitation in a time-domain study. The response per volt at resonance (resonance frequency is indicated) and at 4 kHz of a single speaker and array elements are summarized in Table 1. The smaller response of the array elements is because of the distributed applied power amongst the 16 parallel elements (0 dBm is the maximum power delivered by the signal source). Fig. 8b shows a time domain response of a 2.5 mm single speaker element at 4 kHz to a sinewave actuation. A possible reason for the non-sinusoidal behavior with 10 V AC actuation is the harmonic distortion of the speaker (See the graph without DC bias). This means that when subharmonic stimuli (at 4 kHz) of the resonance frequency (~ 32 kHz) are applied, the system is strongly excited at its higher harmonics. This phenomenon is commonly observed in piezo-MEMS speakers due to asymmetrical nonlinearities [1,28]. To deal with this non-linearity, 5 V DC bias was added on top of 5 V AC signal as DC bias applies a static lateral force to the membrane and tends to keep the membrane steady, reducing the harmonic vibration. Application of DC bias in harmonic distortion measurements is reported in the literature [29] and in our case, 5 V DC bias reduced the harmonic distortion significantly. Hence, all microphone measurements of the single-element speaker and arrays were performed using the 5 V AC signal with 5 V DC bias. The velocities of the 2.5 mm single speaker element correspond to a membrane displacement of ~50 nm/V at 4 kHz and ~ 500 nm/V at resonance (Membrane velocity from Table 1 can be converted to displacement by division with angular frequency). The simulations in Fig. 2b closely corresponded to a membrane displacement at 4 kHz and at the resonance, in response to the 5 V actuation of the fabricated speaker element.

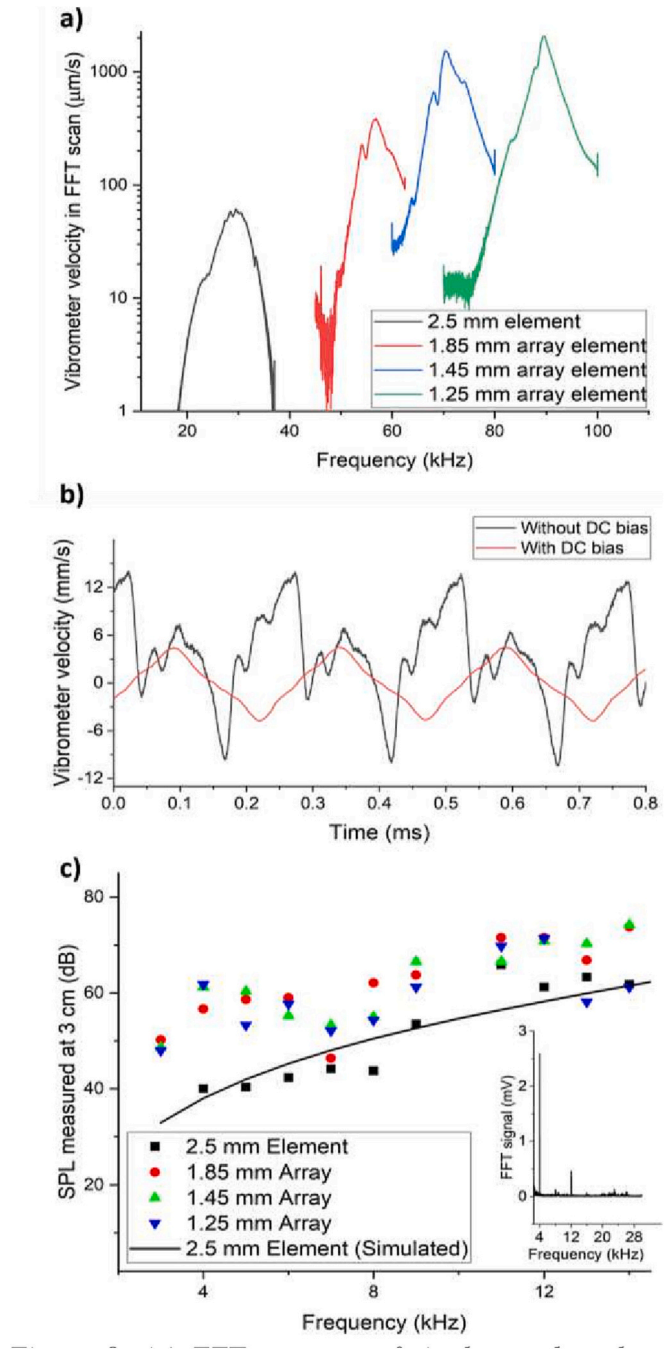

Fig. 8. (a) FFT response of single speaker element and the arrays measured with an LDV system (b) Time domain response of 2.5 mm single speaker element at 4 kHz with 10 V sinewave actuation (black) and with 5 V sinewave actuation on top of 5 VDC (red). (c) Data measured with a microphone and an SPL simulation curve for the 2.5 mm speaker element. Inset shows FFT of the microphone signal at 4 kHz. (For interpretation of the references to colour in this figure legend, the reader is referred to the web version of this article.)

Fig. 8c shows data measured with a microphone (Brüel & Kjær, Type 4192) placed at 3 cm from the speakers and also an SPL simulation curve for the 2.5 mm speaker element at 3 cm for validation. The actuation was with a sinewave of 5 V amplitude on top of 5 V DC bias. Note that the microphone also recorded minimal harmonic distortion with the DC bias applied on top of the 4 kHz AC signal (as shown in FFT in the inset of Fig. 8c). The measurements for the 2.5 mm speaker element, except for a few points, are close to the acoustic pressure simulation curve (within the 6 dB error limit). The figure also shows that the arrays, in general, have performed better in SPL (e.g., a higher response of 1.45 mm array compared to the single element at all recorded points). Although their resonance frequencies are farther from the audible range, the bigger effective apertures result in a higher SPL response. Note that, since the noise in the measurement environment was 20 dB, to maintain the SNR above 10, all the measurements at 3 cm resulting below 40 dB were discarded, including the sub-kHz range measurements. Although measurements at the surface would result in an above 40 dB response, it was not possible to carry out such measurements with high accuracy in positioning the microphone.

A reported analytical study suggests that a 20 µm membrane displacement by an element with a diameter of 2.5 mm at 4 kHz resulted in a 90 dB SPL at 1 cm and the sound pressure generated by the acoustic diaphragm is proportional to vibration amplitude and inversely to the distance [22]. Hence, 0.25 µm displacement at 4 kHz by 2.5 mm element demonstrated in this work translates to 41.5 dB at 3 cm or 51 dB at 1 cm. This is in close agreement with our measurements at 3 cm (40.1 dB from Fig. 8c) and also the simulation at 1 cm (50 dB from Fig. 3b). Also, the surface pressure of 2.5 mm element at 4 kHz is theoretically calculated to be 77 dB which matches the simulation result of 76 dB in Fig. 3b. The surface pressure can approximately be calculated by the product of the membrane velocity (v) of 6 mm/s and the almost reactive acoustic impedance given by $0.8 \cdot ka \cdot \rho c$, where k is the wave number, a is the radius of the membrane, ($ka << 1$ at 4 kHz in-air) [11], ρ and c are the density and acoustic velocity of air, respectively.

6. Conclusion

Low-cost SOI-free fabrication of a piezo-MEMS speaker is proposed, describing speakers realized as a single element as well as in an array. The speaker membrane is made of a 1 µm PZT ring with a 1.5 µm polyimide passive layer on top. LDV characterization has shown the resonance frequency of a single speaker element with a diameter of 2.5 mm to be 30 kHz with a sensitivity of 100 mm/s/V, whereas sensitivity at 4 kHz is around 1.2 mm/S/V. The speaker element can produce around 70–90 dB in-ear Sound Pressure Level (SPL) response in audible frequencies (100 Hz – 10 kHz) at 5 V excitation as shown by a simulation in an ear-coupler which is in line with the LDV measurements. The arrays, on average, have shown a 10 dB higher SPL compared to a single-speaker element as measured by a microphone. Based on the findings, it can be inferred that the technology discussed in this paper is better suited for an earphone application rather than being used as a free-field speaker.

Declaration of Competing Interest

The authors declare that they have no known competing financial interests or personal relationships that could have appeared to influence the work reported in this paper.

Data availability

No data was used for the research described in the article.

Acknowledgments

This work was supported by KU Leuven Interdisciplinary Networks (ID-N) under grant No. ZKD-6578. Also, I would like to acknowledge Yangyang Guan's assistance in conducting the microphone measurements.

References

[1] F. Stoppel, A. Männchen, F. Niekiel, D. Beer, T. Giese, B. Wagner, New integrated full-range MEMS speaker for in-ear applications, in: 2018 IEEE Micro Electro Mechanical Systems (MEMS), Belfast, UK, 2018, pp. 1068–1071, https://doi.org/10.1109/MEMSYS.2018.8346744.

[2] B.M. Diamond, J.J. Neumann, K.J. Gabriel, Digital sound reconstruction using arrays of CMOS-MEMS microspeakers, in: 2002 IEEE Micro Electro Mechanical Systems (MEMS), Las Vegas, NV, USA, 2002, pp. 292–295, https://doi.org/10.1109/MEMSYS.2002.984260.
[3] Haoran Wang, Mengyuan Li, Yuanyuan Yu, Zhenfang Chen, Yingtao Ding, Huabei Jiang, Huikai Xie, A Piezoelectric MEMS Loud Speaker Based on Ceramic PZT, 2019, pp. 857–860, https://doi.org/10.1109/TRANSDUCERS.2019.8808528.
[4] C.B. Eom, S. Trolier-McKinstry, Thin-film piezoelectric MEMS, MRS Bull. 37 (2012) 1007–1017, https://doi.org/10.1557/mrs.2012.273.
[5] Byung-Hun Kim, Hwa-Sun Lee, Sung-Wook Kim, Piljoong Kang, Yoon-Sok Park, Hydrodynamic responses of a piezoelectric driven MEMS inkjet print-head, Sensors Actuators A Phys. 210 (2014), https://doi.org/10.1016/j.sna.2014.02.009.
[6] Yiping Zhu, Wenjing Liu, Kemiao Jia, Wenjun Liao, Huikai Xie, A piezoelectric unimorph actuator based tip-tilt-piston micromirror with high fill factor and small tilt and lateral shift, Sensors and Actuators A Physical. 495-501 (2011), https://doi.org/10.1016/j.sna.2011.03.018.
[7] Gabriel Smith, Ryan Rudy, Don DeVoe, Ronald Polcawich, Integrated thin film piezoelectric traveling wave ultrasonic motor, Sensors Actuators A Phys. 188 (2011) 1464–1467, https://doi.org/10.1109/TRANSDUCERS.2011.5969627.
[8] Matteo Rinaldi, Chiara Zuniga, Chengjie Zuo, Gianluca Piazza, Super-high-frequency two-port AlN contour-mode resonators for RF applications, IEEE Trans. Ultrason. Ferroelectr. Freq. Control 57 (2010) 38–45, https://doi.org/10.1109/TUFFC.2010.1376.
[9] Wang Haoran, Yu Yuanyuan, Chen Zhenfang, Yang Hao, Jiang Huabei, Xie Huikai, Design and Fabrication of a Piezoelectric Micromachined Ultrasonic Transducer Array Based on Ceramic PZT, 2018, https://doi.org/10.1109/ICSENS.2018.8589693.
[10] Lawrence E. Kinsler, Austin R. Frey, Alan B. Coppens, James V. Sanders, Fundamentals of Acoustics, Wiley, United Kingdom, 2000.
[11] Sina Sadeghpour, Michael Kraft, Robert Puers, Design and fabrication strategy for an efficient PZT based piezoelectric micromachined ultrasound transducer (pMUT), J. Micromech. Microeng. 29 (2019), https://doi.org/10.1088/1361-6439/ab4527.
[12] Joontaek Jung, Wonjun Lee, Woojin Kang, EunJung Shin, Jungho Ryu, Hongsoo Choi, Review of piezoelectric micromachined ultrasonic transducers and their applications, J. Micromech. Microeng. 27 (2017), https://doi.org/10.1088/1361-6439/aa851b.
[13] Jeong Yongbin, Genoe Jan, Gijsenbergh Pieter, Segers Jeremy, Heremans Paul, Cheyns David, Fully flexible PMUT based on polymer materials and stress compensation by adaptive frequency driving, Journal of Microelectromechanical Systems (2020) 1–7, https://doi.org/10.1109/JMEMS.2020.3043052.
[14] Gabriel Smith, Jeffrey Pulskamp, Luz Sanchez, Daniel Potrepka, Robert Proie, Tony Ivanov, Ryan Rudy, William Nothwang, Sarah Bedair, Christopher Meyer, Ronald Polcawich, PZT-based piezoelectric MEMS technology, J. Am. Ceram. Soc. 95 (2012) 1777, https://doi.org/10.1111/j.1551-2916.2012.05155.x.
[15] Shih-Hsiung Tseng, Sung-Cheng Lo, Yi-Jia Wang, Shih-Wei Lin, Mingching Wu, Weileun Fang, Sound Pressure and Low Frequency Enhancement Using Novel PZT MEMS Microspeaker Design, 2020, pp. 546–549, https://doi.org/10.1109/MEMS46641.2020.9056291.
[16] J. Zhang, R.J. Perez, E.J. Lavernia, Documentation of damping capacity of metallic, ceramic and metal-matrix composite materials, J. Mater. Sci. 28 (1993) 2395–2404, https://doi.org/10.1007/BF01151671.
[17] D.D.L. Chung, Review: materials for vibration damping, J. Mater. Sci. 36 (2001) 5733–5737, https://doi.org/10.1023/A:1012999616049.
[18] S. Sadeghpour, S.V. Joshi, C. Wang, M. Kraft, Novel phased Array piezoelectric micromachined ultrasound transducers (pMUTs) for medical imaging, IEEE Open Journal of Ultrasonics, Ferroelectrics, and Frequency Control 2 (2022) 194–202, https://doi.org/10.1109/OJUFFC.2022.3207128.
[19] G. Massimino, C. Gazzola, V. Zega, S. Adorno, A. Corigliano, Ultrasonic Piezoelectric Mems Speakers for in-Ear Applications: Bubbles-like and Pistons-like Innovative Designs, 2022 23rd International Conference on Thermal, Mechanical and Multi-Physics Simulation and Experiments in Microelectronics and Microsystems (EuroSimE), St Julian, Malta, 2022, pp. 1–4, https://doi.org/10.1109/EuroSimE54907.2022.9758884.
[20] Cenk Acar, Andrei Shkel, MEMS Vibratory Gyroscopes: Structural Approaches to Improve Robustness, Springer, Germany, 1979.
[21] Generic 711 Coupler — An Occluded Ear-Canal Simulator. Available online: https://www.comsol.com/model/generic-711-coupler-8212-an-occluded-ear-canal-simulator-12227. (accessed on 20 January 2023).
[22] Haoran Wang, Yifei Ma, Qincheng Zheng, Ke Cao, Yao Lu, Huikai Xie, Review of recent development of MEMS speakers, Micromachines. 12 (2021) 1257, https://doi.org/10.3390/mi12101257.
[23] Haoran Wang, Manish Godara, Zhenfang Chen, Huikai Xie, A one-step residue-free wet etching process of ceramic PZT for piezoelectric transducers, Sensors Actuators A Phys. 290 (2019), https://doi.org/10.1016/j.sna.2019.03.028.
[24] M. Rodríguez-Aranda, Piñar Francisco de Paula, F.J. Espinoza-Beltrán, Flores-Ruiz Francisco, Sarabia Eleazar, Mayen Rodrigo, Yañez Limon Jose, Ferroelectric hysteresis and improved fatigue of PZT (53/47) films fabricated by a simplified sol–gel acetic-acid route, Journal of Materials Science Materials in Electronics. 25 (2014), https://doi.org/10.1007/s10854-014-2237-z.
[25] JBL C50HI in-ear headphones specs retrieved from URL:https://in.jbl.com/in-ear-headphones/JBL+C50HI.html on 20 January 2023.
[26] Phillips TAE1107BK/94 in-ear wired headphones specs, retrieved from URL: https://www.philips.co.in/c-p/TAE1107BK_94/in-ear-wired-headphones on 20 January 2023.
[27] Vivek Rathod, A review of electric impedance matching techniques for piezoelectric sensors, Actuators and Transducers. Electronics. 8 (2019) 169, https://doi.org/10.3390/electronics8020169.
[28] S. Temme, Application Notes - Audio Distortion Measurements (bo0385), Brüel, Kjær, 1992.
[29] Liechti Romain, Stephane Durand, Hilt Thierry, Casset Fabrice, Dieppedale Christel, Colin Mikaël, High performance piezoelectric MEMS loudspeaker based on an innovative wafer bonding process, 2022, https://doi.org/10.21203/rs.3.rs-2080237/v1.